Rapid Communications | Editors' Suggestion

Universal phase diagram of superconductivity and charge density wave versus high hydrostatic pressure in pure and Se-doped $1T$-TaS_2

Bosen Wang,[1,2,3,*] Yu Liu,[4] Xuan Luo,[4] Kento Ishigaki,[3] Kazuyuki Matsubayashi,[5] Wenjian Lu,[4] Yuping Sun,[6,4,7,†] Jinguang Cheng,[1,2] and Yoshiya Uwatoko[3,‡]

[1]*Beijing National Laboratory for Condensed Matter Physics and Institute of Physics, Chinese Academy of Sciences, Beijing 100190, China*
[2]*School of Physical Sciences, University of Chinese Academy of Sciences, Beijing 100190, China*
[3]*Institute for Solid State Physics, University of Tokyo, Kashiwanoha 5-1-5, Kashiwa, Chiba 277-8581, Japan*
[4]*Key Laboratory of Materials Physics, Institute of Solid State Physics, Chinese Academy of Sciences, Hefei 230031, China*
[5]*Department of Engineering Science, University of Electro-Communications, Chofu, Tokyo 182-8585, Japan*
[6]*High Magnetic Field Laboratory, Chinese Academy of Sciences, Hefei 230031, China*
[7]*Collaborative Innovation Center of Advanced Microstructures, Nanjing University, Nanjing, 210093, China*

(Received 26 November 2017; revised manuscript received 11 April 2018; published 25 June 2018)

The coexistence of superconductivity (SC) and charge density waves (CDWs) was investigated for pure and Se-doped $1T$-TaS_2 via electrical resistivity under hydrostatic pressure. A universal superconducting phase diagram was revealed on the border of CDWs. Unlike isovalent S/Se doping and uniaxial pressure, the application of high hydrostatic pressure suppresses CDW more sensitively and thoroughly with the critical pressures $P_c(x) \sim 4.70$–6.55 GPa. A pressure-induced superconducting state coexists with various CDWs, then bulk SC emerges along with the complete collapse of various CDWs. The superconducting transition temperature increases monotonously up to ~7.3 K at 15 GPa without a domelike shape. The results clarify that the superconducting Cooper pairing is associated with the CDWs' instability near $P_c(x)$. Above $P_c(x)$, the monotonous increase of T_c is attributed to different evolutions of the electronic structures and phonon vibration spectra under hydrostatic and uniaxial pressures and a further inhibition of undetected CDWs.

DOI: 10.1103/PhysRevB.97.220504

The competition, coexistence, and interplay of charge density waves (CDWs) and superconductivity (SC) have been intensively studied in low-dimensional electronic systems [1–5]. In a stable CDW state, the periodic modulations of lattices and electrons open gaps along with enhanced electron-phonon couplings [1,2]. Considering electron-electron correlations, the interplay of CDWs and SC becomes complex and unpredictable. For example, various phase diagrams concerning SC and CDWs have been constructed in layered transition-metal dichalcogenides (TMDs) versus the external parameters [3–8]. But whether or not superconducting pairing belongs to an unconventional mechanism is still under debate even after many years of extensive efforts. These diagrams are not universal because they rely on various factors such as lattice symmetry, band structures, and electronic correlations, and thus contradictory arguments regarding CDWs and SC are still being made [9–12].

$1T$-TaS_2 exhibits several interesting phases including CDWs, a Mott insulating state, and SC when subjected to external stimuli [6,9–11,13]. At ambient pressure (AP), $1T$-TaS_2 undergoes three successive transitions: a metallic state to an incommensurate CDW (ICCDW) at $T_{ICCDW} = 550$ K, to a nearly commensurate CDW (NCCDW) at $T_{NCCDW} = 350$ K, and then to a commensurate CDW (CCDW) at $T_{CDW} = 190$ K; below T_{CDW}, a Mott insulating state develops with a band gap ~0.2 eV [11,13]. SC can be induced and coexists with CDW via chemical substitutions in $1T$-TaS_2 [14–17]. For example, the substitution of Fe by Ta melts the Mott/CDW state by weakening the Anderson localization of electrons. At low temperatures, a dome-shaped SC with a $T_c^{max} \sim 2.1$ K emerges, which was due to the formation of a new electron pocket in the center of the Brillouin zones [15,18]. In the case of the substitution of Se by S, the Mott state melts and SC appears, but the CDW phase transition temperatures are insensitive to chemical doping [14]. It implies that the substitution of Se by S does not act as "chemical pressure" but the S/Se disorders play an important role [6]. It should be noted that bulk SC is hard to achieve in these samples because the CDW is robust, which differs from the cases of $2H$-TMDs [3,6,19]. In contrast, the application of high pressure that does not introduce any disorder is effective to manipulate CDWs and derives interesting phase diagrams in TMDs [3,5,11,12,16]. For example, $1T$-$TiSe_2$ exhibits pressure-induced domelike SC with $T_c^{max} = 1.8$ K, and an unconventional pairing mechanism was suggested considering the indispensable hybridizations of phonons and other exciton modes [20]. For isostructural $1T$-TaS_2, high pressure suppresses the Mott state and SC can coexist with NCCDW. The onset of the superconducting transition temperature T_c^{onset} increases with pressures up to ~7 GPa, but remains ~5 K at elevated pressures [11,21]. To understand the observed phase diagram for $1T$-TaS_2 has been challenging because the usual domelike SC is absent [5,20,22,23]. SC has been thought to be an effect of unconventional pairing, but

*bswang@iphy.ac.cn
†ypsun@issp.ac.cn
‡uwatoko@issp.u-tokyo.ac.jp

CDW is argued to be weakly connected with conventional SC by thinning $1T$-TaS_2 at AP, which seems to be consistent with previous investigations [9,24,25]. The mechanism of pressure-induced SC remains elusive. In addition, previous studies also did not clarify whether there is a zero-resistivity state and bulk SC in pressurized $1T$-TaS_2. Another factor contributing to the divergence is that the available experiments were performed in uniaxial pressure cells [5,11,22]. Since more and more experimental studies revealed discrepancies under hydrostatic and/or uniaxial pressures [26–28], it is thus necessary to reexam the intrinsic pressure effect and to establish the phase diagram of $1T$-TaS_2 under high hydrostatic pressures.

Both $1T$-TaS_2 and $1T$-$TaSe_2$ crystallize in a CdI_2-type structure (space group $P\bar{3}m1$). Ta atoms form star-of-David clusters with a $\sqrt{13} \times \sqrt{13}$ superlattice in the Mott insulating state [13,14]. Their electronic structures have been predicted to be similarly featured by the Ta-5d band energy gaps arising from electronic localizations, but their different electrical transports are puzzling [13,14,29]. Based on previous investigations, we are encouraged to reexam the underlying mechanism of pressured-induced SC in $1T$-TaS_2 under hydrostatic pressure. A comparison study on the "chemical pressure" versus "hydrostatic physical pressure" will allow us to acquire a better understanding of the interplay of CDWs and SC. In this Rapid Communication, we will uncover universal phase diagrams of SC and CDWs for pure and Se-doped $1T$-TaS_2, which are different from the results under uniaxial pressure.

High-quality $1T$-$TaS_{1-x}Se_x$ ($x = 0$, 0.8, 1.0, 2.0) single crystals were grown by the chemical vapor transport method [14]. Single-crystal x-ray diffraction (XRD) was performed to verify phase purity. High-pressure resistivity measurements were performed in a cubic anvil cell apparatus, which can generate hydrostatic pressures up to 15 GPa; a preheated MgO cube was used as the gasket and glycerin was the pressure transmitting medium [26,27]. Resistivity was measured by using the standard four-probe method with current applied within the ab plane. All the experiments were performed in a ^{4}He refrigerator cryostat ($1.9\,\mathrm{K} \leqslant T \leqslant 300\,\mathrm{K}$).

Figure 1 shows the temperature-pressure-composition phase diagram for $1T$-$TaS_{1-x}Se_x$. With increasing Se content at AP, the CCDW in $1T$-TaS_2 transits into NCCDW at $x = 0.5$, and then to CCDW again in $1T$-$TaSe_2$, with the transition temperature increasing from 350 K in $1T$-TaS_2 to 473 K in $1T$-$TaSe_2$ [14,28]. The ground state evolves from a Mott state through a domelike SC region, and then to a metallic state. It is unexpected because the Mott insulator appears in $1T$-TaS_2 with a smaller unit-cell volume, while the SC here is induced via enlarging the unit-cell volume. Such abnormal behavior induced by "negative chemical pressure" implies that the unit-cell volume is not the principal parameter for the present diagrams. In contrast, the application of high "physical" pressure suppresses both CCDW and NCCDW; both transitions collapse near the critical pressures $P_c(x)$; bulk SC appears above $P_c(x)$ with a simple metallic behavior in the normal state. In striking contrast, the NCCDW is very robust in the normal state above the SC dome of $1T$-$TaS_{1-x}Se$. With increasing pressure, the coexistence of SC and CDW is evident. For all samples, the superconducting transition temperatures increase monotonously with pressure until 15 GPa, with the maximal T_c^{max} reaching ~7.3 K on the S-rich side and ~5.3 K

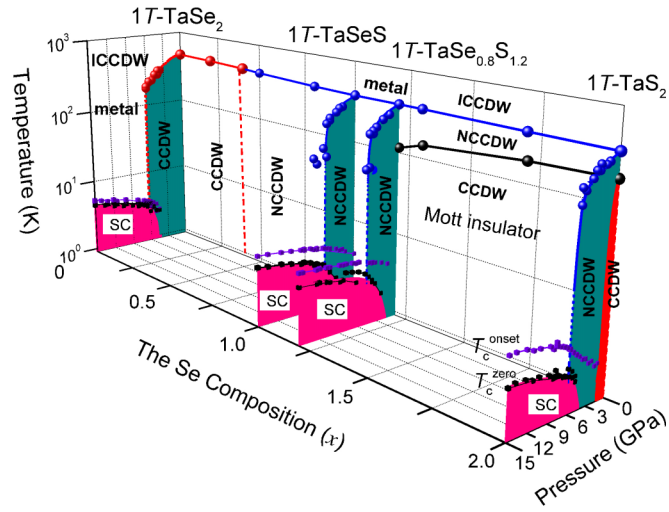

FIG. 1. Phase diagram of $1T$-$TaS_{2-x}Se_x$ vs temperature, pressure, and S/Se composition. The red dashed line separates the CCDW and the NCCDW; the cyan-colored lines indicate the pressure dependence of T_{CCDW} and T_{NCCDW} by a classical mean-field model; the lines across data points imply trends.

on the Se-rich side, which are higher than that of $1T$-$TaS_{1-x}Se_x$ (~3.6 K) at AP [14]. These comparisons underscore the distinct effects of chemical pressure versus hydrostatic pressure. The volume shrinks ~11.6% from $1T$-$TaSe_2$ to $1T$-TaS_2 (a, b contracts ~3.1%, c ~ 5.9%), smaller than the decrease ~5.6% at 6.5 GPa [14]. It implies that phase diagrams of this system strongly rely on the tuning routes [6,21]. It should be noted that a similar temperature-pressure phase diagram of $1T$-TaS_2 has been explored in a diamond anvil pressure cell (DAC) with helium as the pressure-transmitting medium (PTM) [21]. But the T_c value increases and reaches a nearly constant of 5 K, which is similar with the case using solid NaCl as the PTM [11]. Its origin remains confusing.

Figure 2 shows the temperature dependence of resistivity $\rho(T)$ for $1T$-TaS_2 under various hydrostatic pressures up to 15 GPa. At AP, two sudden resistivity jumps are observed at ~350 and ~190 K, corresponding to the successive transitions from ICCDW to NCCDW and then to the CCDW state, respectively. Their transition temperatures T_{NCCDW} and T_{CCDW} in Figs. 2 and 3 are determined from the maximum of $d\rho/dT$. The CCDW disappears at 1.5 GPa, and the ICCDW-NCCDW transition shifts progressively to low temperatures and broadens up with increasing P, reflecting that lattice contraction exacerbates the NCCDW instability [28]. At 6.0 GPa, no detectable jump in $\rho(T)$ implies the collapse of NCCDW. The magnitude of $\rho(T)$ decreases with similar temperature dependences in the pressure ranges of 1.5–5.5 and 6–15 GPa. Remarkably, $\rho(T)$ at 15 GPa reduces by ~20000 times (<190 K) and ~20 times (190–350 K) compared to that at AP. Such a change should be attributed to the delocalization of electrons because of the closure of the CDW band gaps [11,18]. The results are reproducible and confirmed in four independent runs. Similar measurements were performed for $x = 0.8$, 1.0, and 2.0 to track the evolutions of the CDW transitions. As shown in Figs. S1–S3 of the Supplemental Material [30], the results are in general similar, except for some details, such as $P_c(x)$, the magnitude of jumps in $\rho(T)$, and the T_c^{max}.

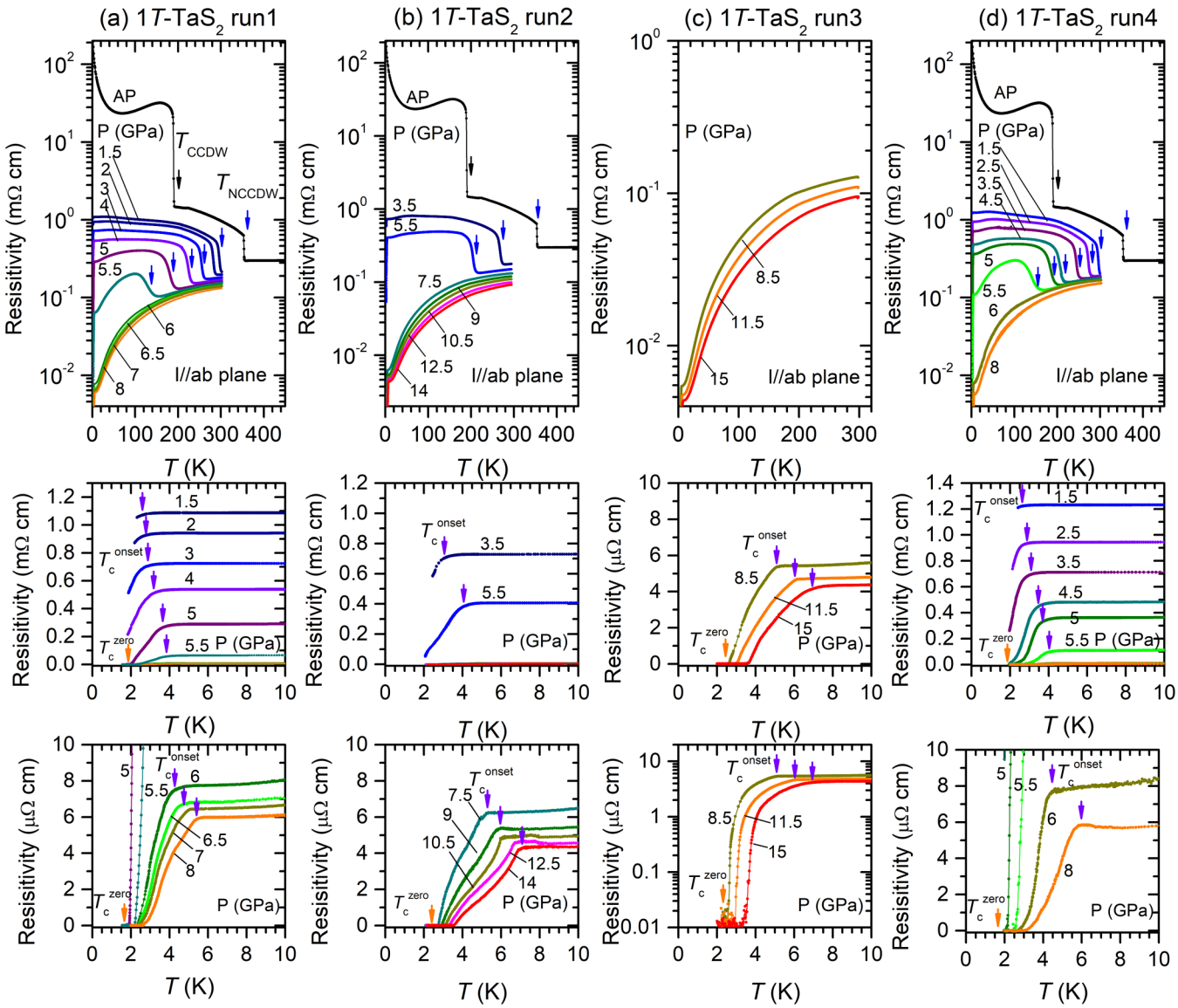

FIG. 2. Temperature dependence of $\rho(T)$ of $1T$-TaS_2 under various pressures up to 15 GPa. The arrows indicate phase transitions: the CCDW-NCCDW transition (black), the NCCDW-ICCDW transition (blue), the onset superconducting transition T_c^{onset} (purple), and the zero-resistivity state temperature T_c^{zero} (yellow).

For $x = 0.8$, 1.0, and 2.0, T_{NCCDW} at AP increases gradually to 379, 390, and 473 K, respectively. Under pressure, T_{NCCDW} decreases to ~300 K at 1.5 GPa for $x = 0.8$, and 1.0, lower than that of $1T$-$TaSe_2$ (~400 K). The critical pressure $P_c(x)$ is ~4.5 GPa for $x = 0.8$ and 1.0, and then increases to ~6.5 GPa for $x = 2.0$. This means that the CDW state in $1T$-TaS_2 and $1T$-$TaSe_2$ is more robust. Interestingly, $\rho(T)$ shows a plateau around 75 K at 4.5 and 5.0 GPa (run 1), 4.0 GPa (run 2) for $x = 0.8$, and 4.5 and 5.0 GPa (run 2) for $x = 1.0$, which indicates the appearance of a phase transition. Whether it is a new CDW transition or related to the S/Se disorder-related behaviors needs to be confirmed. The magnitude of $\rho(T)$ at 15 GPa was reduced compared to that at AP as 120 (<120 K), 25 (<390 K), and ten times (<473 K) for $x = 0.8$, 1.0, and 2.0, respectively. It implies that the CDW gaps are reduced and the interlayer couplings are strengthened by Se doping [14,28].

Low-T $\rho(T)$ is plotted for $1T$-TaS_2 in the lower panels of Fig. 2. Along with the suppression of CCDW, a drop appears ~2.4 K at 1.5 GPa as a sign of SC [11]. T_c^{onset} and T_c^{zero} are defined as the temperatures where $\rho(T)$ starts to drop and reaches zero, respectively. The drop gets more evident as P increases and T_c^{onset} increases, concomitant with the suppression of NCCDW. At 5.0 GPa, T_c^{zero} is ~1.9 K, and increases monotonically. At 15 GPa, T_c^{onset} and T_c^{zero} are ~7.3 and ~3.7 K, respectively. With increasing P, a slope change for both $T_c^{onset}(P)$ and $T_c^{zero}(P)$ can be found at $P_c(x)$ in Fig. 3(a). Above $P_c(x)$, the pressure coefficients dT_c^{onset}/dP and dT_c^{zero}/dP are ~0.336(6) and ~0.143(1) K/GPa, respectively. For the Se-doped samples, the pressure dependences of T_c^{onset} and T_c^{zero} are shown in Figs. 3(b)–3(d). Both T_c^{onset} and T_c^{zero} increase with pressure and reach maxima at 15 GPa, i.e., ~6.8 and ~4.6 K for $x = 0.8$, ~ 6.9, and ~4.9 K for $x = 1.0$, and ~5.3 and ~4.6 K for $x = 2.0$. In comparison,

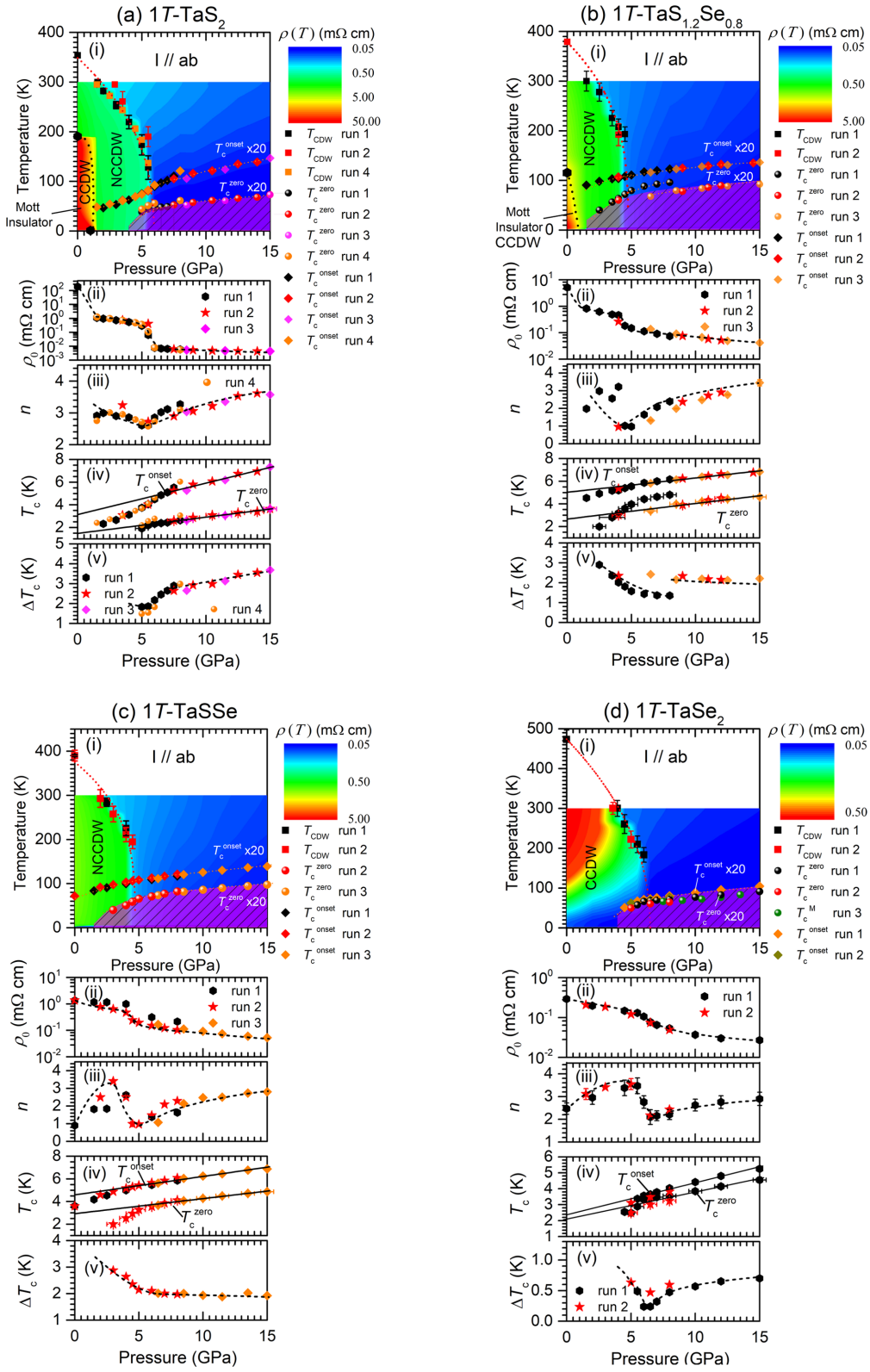

FIG. 3. The parameters as a function of pressure: (i) the temperature-pressure diagram, (ii) the residual resistivity ρ_0 by fitting $\rho = \rho_0 + AT^n$ (from just above T_c to 20 K), (iii) the exponent n, (iv) T_c^{onset} and T_c^{zero}, and (v) ΔT_c (defined as $T_c^{onset} - T_c^{zero}$); the black lines in (iv) are linear fittings and the yellow dashed lines indicate trends.

$T_c \sim 7.3$ K of TaS_2 is the highest among 1T-TMDs [4–11]. For example, the maximum T_c^{onset} is ~4.2 K for Cu_xTiSe_2 ($x \sim 0.08$) [4], ~1.8 K for 1T-$TiSe_2$ under P [5], ~3.0 K for 1T-$TiSe_2$ under electrical field [7], and ~5 K in 1T-TaS_2 under P [11]. However, in most cases the zero-resistivity state cannot be achieved. The coefficients dT_c^{onset}/dP (dT_c^{zero}/dP)

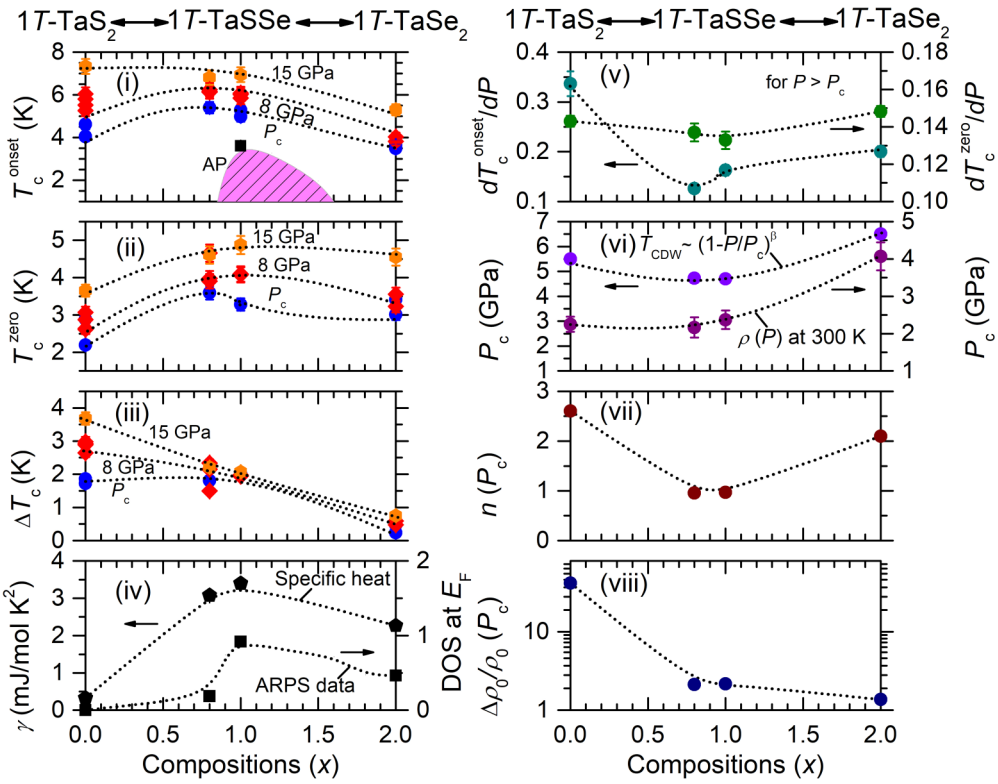

FIG. 4. The related parameters are compared vs the Se content: (i) T_c^{onset}, (ii) T_c^{zero}, (iii) ΔT_c, (iv) the electronic coefficient γ, and the density of states at the Fermi level DOS (E_F), (v) the pressure coefficients dT_c^{onset}/dT, dT_c^{zero}/dT, (vi) the critical pressure $P_c(x)$, (vii) the exponent n at P_c, and (viii) the normalized $\Delta\rho/\rho_0(P_c)$; the dashed lines indicate trends.

are ~0.126(1)[~0.137(1)] K/GPa, ~0.162(9) [~0.132(8)] K/GPa, and ~0.200(5) [~0.148(3)] K/GPa for $x = 0.8$, 1.0, and 2.0, respectively. We note that dT_c^{onset}/dP (dT_c^{zero}/dP) reaches a minimum at $x = 0.8$ and 1.0 while T_c^{onset} (T_c^{zero}) becomes maximum, which means that T_c is not sensitive to pressure for the superconducting samples [21]. As reported, a large diamagnetic response below T_c has been observed in 1T-$TaSe_2$ just above $P_c(x)$ [28], which is evidence of the coexistence of SC and CDW at a narrow pressure interval. A zero-resistivity superconducting state appears but the CDW transition is high, which implies that some superconducting channels form and coexist with CDW domain walls [11,21,28].

Temperature-pressure phase diagrams are plotted in Figs. 3(a)–3(d). For each sample, the pressure dependences of T_{CCDW} and T_{NCCDW} are well fitted by the classical mean-field quantum fluctuation model as T_{CCDW} (or T_{NCCDW}) = $T(\mathrm{AP})|1 - P(x)/P_c(x)|^{\beta(x)}$, where T(AP), $P_c(x)$, and $\beta(x)$ represent the estimated T_{CDW} at AP, the critical pressure when T_{CDW} decreases to zero, and an exponent characterizing the suppression of order parameters [5,22,31]. For $x = 0$, 0.8, 1.0, and 2.0, T(AP) is 348.5, 377.9, 376.5, and 473.5 K, which are identical to the T_{CCDW} (or T_{NCCDW}), and $P_c(x)$ is 5.52(2), 4.75(9), 4.70(2), and 6.55(2) GPa, respectively. The parameter $\beta(x)$ is 0.334(4), 0.328(2), 0.302(7), and 0.466(2). We note that β is smaller than that of 1T-TaS_2 ($\beta \sim 1$) under uniaxial pressure [11,21], but the model is similar to those of 1T-$TiSe_2$ ($\beta \sim 0.87$) [5] and $o - TaS_3$ ($\beta \sim 0.5$) [31]. It means that CCDW and NCCDW changes more sensitively under hydrostatic pressure and CDW correlation lengths are different from previous reports. $P_c \sim 5.52$ GPa in 1T-TaS_2 is consistent with theoretical calculations (~5 GPa) [29], but is ~1.5 GPa lower than the experiments, ~7 GPa [11], whereas $P_c \sim 6.55$ GPa in 1T-$TaSe_2$ is five times smaller than the theoretical prediction of ~30 GPa [28,29].

To understand the relationship between CDW and SC, normal-state resistivity is analyzed by $\rho = \rho_0 + A \times T^n$ and $\ln \Delta\rho(= \rho - \rho_0) \sim \ln T$, where ρ_0 is the residual resistivity, and the coefficient A and the exponent n are related to inelastic electron scatterings. For a conventional Fermi liquid, $n = 2$ and a departure from $n = 2$ can be well interpreted in terms of the change of the electron-electron correlation effect. n is estimated by fitting the data in the temperature range from T_c to 20 K. For each x, ρ_0 reduces as P increases and experiences a faster reduction at $P_c(x)$ where A reaches a maximum. At ambient P, the exponent n(AP) is 1.97, 0.90, and 2.5 for $x = 0.8$, 1.0, and 2.0. Under pressure, n initially increases slightly, decreases to a minimum, and then increases to ~3.0 at 15 GPa. At $P_c(x)$, n is ~2.61 and 2.09 for $x = 0$ and 2.0, and decreases to ~0.96 for $x = 0.8$ and 1.0, contrary to the shape of the SC dome. These characteristics imply that SC enhances with a smaller n [5,28]. Unlike the empirical electron-electron scattering $n = 2$, the decrease of n here is unusual [13]. In two-dimensional (2D) 1T-$TiSe_2$, a sizable suppression ($n = 3$ at AP to $n \sim 2.6$ in the range of 2–4 GPa) emerges near a collapsed CDW, which is evidence of CDW fluctuations [5]. To a certain extent, the evolution of the exponent n can be seen as evidence of CDW fluctuations in various reported systems

because of the concomitant electron-electron and electron-phonon scatterings [5,13,28]. Based on these, the decrease of n should be attributed to the evidence of CDW fluctuations. In Figs. 3(a)–3(d), the pressure dependences of $\rho_0, n, T_c^{onset}, T_c^{zero}$, and ΔT_c ($= T_c^{onset} - T_c^{zero}$) are plotted. At first, both T_c^{onset} and T_c^{zero} increase, but with different pressure coefficients. As a result, ΔT_c of 1T-TaS_2 and 1T-$TaSe_2$ shows a trough with a minimum of ∼1.83 and ∼0.24 K at $P_c(x)$, and then increases further up to 15 GPa, while for $x = 0.8$ and 1.0, ΔT_c initially decreases and tends to saturation above $P_c(x)$. It indicates that SC in 1T-TaS_2 and 1T-$TaSe_2$ may not be the same for the doped samples. At $P_c(x)$, ΔT_c is ∼1.80 K for $x = 0$, 0.8, and 1.0, higher than that of 1T-$TaSe_2$ (∼0.5 K), while at 15 GPa, ΔT_c increases up to ∼3.68, ∼ 2.20,∼2.07, and ∼0.75 K for $x = 0$, 0.8, 1.0, and 2.0. We note that ΔT_c of 1T-TaS_2 is more sensitive to pressure than the other three. One possible reason is that S/Se atomic disorder broadens the superconducting transitions [14]. Whether this behavior is related to dimensionality and other factors remains unclear. Using the ρ_0 and $P_c(x)$, the magnitude of jump in $\rho(T)$ can be defined as $\Delta\rho/\rho_0(P_c)$ as in Fig. 4(viii). Its value decreases from ∼36 ($x = 0$) to 2 ($x = 0.8$ and 1.0) and 1($x = 2.0$), which can be explained as an enhancement of interlayer coupling [28]. Interestingly, both T_c^{onset} and T_c^{zero} show a domelike dependence of the Se content at $P_c(x)$, 8 GPa, and 15 GPa in Figs. 4(i)-4(iii). As shown in Fig. S4 [30], specific heat was fitted by using $C = \gamma T + \beta T^3$, where the former and latter are the electron and phonon contributions, respectively. The electronic coefficient γ was found to increase from 0.325(1) for $x = 0$ to 3.396(3) mJ/mol K for $x = 1.0$, which is consistent with the density of states (DOS) at the Fermi level by angle-resolved photoemission spectroscopy (ARPES) [18]. Combined with these features and previous reports [14,28,29], we suspect that anisotropic SC in 1T-TaS_2 is different from that of 1T-$TaSe_2$. On this issue, further studies on SC versus different magnetic fields under pressure can give us the details. As above, a universal phase diagram is revealed on the border of CDW versus hydrostatic pressure. Bulk SC appears after complete CDW collapse, implying the competition between SC with CDW [1,2]. High pressure reshapes the electronic structures and electron-phonon couplings, which usually causes an enhanced DOS (E_F) and an instability of phonon vibration modes [32]. As mentioned above, the sample contains superconducting channels and CDW domain walls [21,28]. This model can explain the coexistence of zero resistance SC and higher CDW transition temperatures, and the superconducting shielding volume in 1T-$TaSe_2$ is ∼65% above $P_c(x)$ [28]. Finally, we discuss briefly the monotonic increase of T_c with pressure. Usually, in an overdoped superconducting region of a domelike SC diagram, enhanced impurity scatterings are dominant and the electron-phonon couplings will reduce when they are far from CDWs, which can explain the reduction of T_c. Here, the monotonic increase of T_c may be related to the evolutions of the phonon vibration modes which can enhance T_c. It was supported by theoretical predictions [14,29,32]. Second, hidden CDWs cannot be detected by electrical transport measurement, and their further suppression by pressure may cause an increase of T_c [11,21,28,33]. One example is the absence of 100% bulk SC in 1T-Cu_xTiSe_2 because of an undetected ICCDW [33]. Third, nonhydrostatic pressure inevitably induces pressure distributions [22,28]. An immediate consequence is the distinct evolutions of the electronic structures and phonon spectra under hydrostatic and uniaxial pressures even from the same starting point. Thus, the different phase diagram is due to this factor [34].

We thank S. Nagasaki for technical assistance and Dr. J. Gouchi, Professor G. H. Cao, and Dr. L. J. Li for useful discussions. This work is supported by the National Key Research and Development Program of China (2016YFA0300404), The Strategic Priority Research Program and Key Research Program of Frontier Sciences of the Chinese Academy of Sciences (XDB07020100, QYZDB-SSW-SLH013), The National Nature Science Foundation of China (11674326, 11774351, and 11574377), Joint Funds of the National Natural Science Foundation and CAS' Large-scale Scientific Facility (U1232139), a JSPS fellowship for foreign researchers (15F15023), IOP Hundred-Talent Program (Y7K5031X61), and the Youth Promotion Association, CAS (2018010).

B.W., Y.L., X.L, and K. I. contributed equally to this work.

[1] G. Grüner, Rev. Mod. Phys. **60**, 1129 (1988).
[2] A. M. Gabovich, A. I. Voitenko, J. F. Annett, and M. Ausloos, Supercond. Sci. Technol. **14**, R1 (2001).
[3] H. Suderow, V. G. Tissen, J. P. Brison, J. L. Martinez, and S. Vieira, Phys. Rev. Lett. **95**, 117006 (2005).
[4] E. Morosan, H. W. Zandbergen, B. S. Dennis, J. W. G. Bos, Y. Onose, T. Klmczuk, A. P. Ramirez, N. P. Ong, and R. J. Cava, Nat. Phys. **2**, 544 (2006).
[5] A. F. Kusmartseva, B. Sipos, H. Berger, L. Forro, and E. Tutis, Phys. Rev. Lett. **103**, 236401 (2009).
[6] Y. Liu, D. F. Shao, L. J. Li, W. J. Lu, X. D. Zhu, P. Tong, R. C. Xiao, L. S. Ling, C. Y. Xi, L. Pi, H. F. Tian, H. X. Yang, J. Q. Li, W. H. Song, X. B. Zhu, and Y. P. Sun, Phys. Rev. B **94**, 045131 (2016).
[7] L. J. Li, E. C. T. O'Farrell, K. P. Loh, G. Eda, B. Ozyilmaz, and A. H. Castro Neto, Nature (London) **529**, 185 (2016).
[8] J. T. Ye, Y. J. Zhang, R. Akashi, M. S. Bahramy, R. Arita, and Y. Iwasa, Science **338**, 1193 (2012).
[9] Y. Yu, F. Y. Yang, X. F. Lu, Y. J. Yan, Y. H. Cho, L. G. Ma, X. H. Niu, S. Kim, Y. W. Son, D. L. Feng, S. Y. Li, S. W. Cheong, X. H. Chen, and Y. B. Zhang, Nat. Nanotechnol. **10**, 270 (2015).
[10] M. Yoshida, R. Suzuki, Y. Zhang, M. Nakano, and Y. Iwasa, Sci. Adv. **1**, e1500606 (2015).
[11] B. Sipos, A. Kusmartseva, A. Akrap, L. F. H. Berger, and E. Tutis, Nat. Mater. **7**, 960 (2008).
[12] R. Yomo, K. Yamaya, M. Abliz, M. Hedo, and Y. Uwatoko, Phys. Rev. B **71**, 132508 (2005).
[13] J. A. Wilson, F. J. Di Salvo, and S. Mahajan, Phys. Rev. Lett. **32**, 882 (1974).
[14] Y. Liu, R. Ang, W. J. Li, W. H. Song, L. J. Li, and Y. P. Sun, Appl. Phys. Lett. **102**, 192602 (2013).

[15] L. J. Li, W. J. Lu, X. D. Zhu, Z. Qu, L. S. Ling, and Y. P. Sun, Europhys. Lett. **97**, 67005 (2012).
[16] P. D. Hambourger, Solid State Commun. **35**, 405 (1980).
[17] H. X. Luo, W. W. Xie, J. Tao, H. Inour, A. Gyenis, J. W. Krizan, A. Yazdani, Y. M. Zhu, and R. J. Cava, Proc. Natl. Acad. Sci. USA **112**, 1174 (2015).
[18] R. Ang, Y. Tanaka, E. Ieki, K. Nakayama, T. Sato, L. J. Li, W. J. Lu, Y. P. Sun, and T. Takahashi, Phys. Rev. Lett. **109**, 176403 (2012).
[19] D. C. Freitas, P. Rodiere, M. R. Osorio, E. Navarro-Moratalla, N. M. Nemes, V. G. Tissen, L. Cario, E. Coronado, M. Garcia-Hernandez, S. Vieira, M. Nunez-Regueiro, and H. Suderow, Phys. Rev. B **93**, 184512 (2016).
[20] M. Maschek, S. Rosenkranz, R. Hott, R. Heid, M. Merz, D. A. Zocco, A. H. Said, A. Alatas, G. Karapetrov, S. Zhu, J. vanWezel, and F. Weber, Phys. Rev. B **94**, 214507 (2016).
[21] T. Ritschel, J. Trinckauf, G. Garbarino, M. Hanfland, M. v. Zimmermann, H. Berger, B. Buchner, and J. Geck, Phys. Rev. B **87**, 125135 (2013).
[22] Y. I. Joe, X. M. Chen, P. Ghaemi, K. D. Finkelstein, G. A. de la Pena, Y. Gan, J. C. T. Lee, S. Yuan, J. Geck, G. J. MacDougall, T. C. Chiang, S. L. Cooper, E. Fradkin, and P. Abbamonte, Nat. Phys. **2**, 421 (2014).
[23] R. Samnakay, D. Wickramaratne, T. P. Pope, R. K. Lake, T. T. Salguero, and A. A. Balandin, Nano Lett. **15**, 2965 (2015).
[24] S. Y. Li, G. Wu, X. H. Chen, and L. Taillefer, Phys. Rev. Lett. **99**, 107001 (2007).
[25] J. Kacmarcik, Z. Pribulova, V. Paluchova, P. Szabo, P. Husanikova, G. Karapetrov, and P. Samuely, Phys. Rev. B **88**, 020507(R) (2013).
[26] N. Mori *et al.*, High Pressure Res. **24**, 225 (2004).
[27] J.-G. Cheng, K. Matsubayashi, S. Nagasaki, A. Hisada, T. Hirayama, M. Hedo, H. Kagi, and Y. Uwatoko, Rev. Sci. Instrum. **85**, 093907 (2014).
[28] B. S. Wang, Y. Liu, K. Ishigaki, K. Matsubayashi, J. G. Cheng, W. J. Lu, Y. P. Sun, and Y. Uwatoko, Phys. Rev. B **95**, 220501(R) (2017).
[29] Y. Z. Ge and A. Y. Liu, Phys. Rev. B **82**, 155133 (2010); A. Y. Liu, *ibid.* **79**, 220515(R) (2009).
[30] See Supplemental Material at http://link.aps.org/supplemental/10.1103/PhysRevB.97.220504 for resistivity $\rho(T)$ of $1T$-$TaS_{1.2}Se_{0.8}$, $1T$-TaSSe, $1T$-TaS_2 under various pressures up to 15 GPa and specific heat analysis at low temperature.
[31] M. Monteverde, J. Lorenzana, P. Monceau, and M. Nunez-Regueiro, Phys. Rev. B **88**, 180504 (2013).
[32] W. L. McMillan, Phys. Rev. **167**, 331 (1968); L. R. Testardi, Rev. Mod. Phys. **47**, 637 (1975).
[33] A. Kogar, G. A. de la Pena, S. Lee, Y. Fang, S. X.-L. Sun, D. B. Lioi, G. Karapetrov, K. D. Finkelstein, J. P. C. Ruff, P. Abbamonte, and S. Rosenkranz, Phys. Rev. Lett. **118**, 027002 (2017).
[34] R. C. Xiao, W. J. Lu, D. F. Shao, J. Y. Li, M. J. Wei, H. Y. Lv, P. Tong, X. B. Zhu, and Y. P. Sun, J. Mater. Chem. C **5**, 4167 (2017).